

that did not colocalize with these aggregates (Fig. 4B), consistent with the prion-like behavior described for certain RNA binding proteins when dislocated to the cytoplasm (25). Importin  $\alpha$ -1 and importin  $\alpha$ -3 were also mislocalized to cytoplasmic  $\beta$ -protein aggregates (fig. S10, A and B).

Besides THOC, the  $\beta$ -protein interactome in primary neurons contained splicing factors and several other RNA binding proteins (Fig. 4A and table S1), suggesting that the cytoplasmic aggregates affect not only mRNA export, but also nuclear mRNA processing. Indeed, cells containing cytoplasmic aggregates exhibited a more pronounced accumulation of mRNA in the nucleus than cells in which THOC2 was down-regulated (fig. S10C) (26).

Our findings provide insight into common mechanisms that are likely to contribute to aggregate toxicity in neurodegenerative diseases and other disorders. Cytoplasmic aggregates of artificial  $\beta$ -sheet proteins and authentic disease proteins caused a pronounced impairment of nucleocytoplasmic transport and a redistribution of nuclear shuttle factors to the cytosol. Several of these transport proteins, including THOC2 (fig. S11), contain disordered and low-complexity sequences that may render them vulnerable to interactions with the interactive surfaces of cytoplasmic aggregates (table S2). Thus, the inhibition of nuclear transport observed in this system can be assigned to proteotoxicity, rather than to aberrant interactions between RNA repeat sequences and RNA binding proteins (10). Such repeat RNAs occur in the coding region or in untranslated regions of disease genes and are associated with amyotrophic lateral sclerosis, frontotemporal dementia, and CAG repeat disorders (11). Their coexistence with protein aggregates has confounded the analysis of toxicity mechanisms (10, 27, 28).

Surprisingly, otherwise identical aggregation-prone proteins did not interfere with nucleocytoplasmic transport when directed to the nucleus. How the nuclear environment alters the interaction properties of the  $\beta$  proteins remains to be investigated in detail, but our findings suggest that the negatively charged, nucleolar protein NPM1 is involved in shielding interactive aggregate surfaces. Indeed, recent reports that misfolded cytoplasmic proteins are actively imported into the nucleus for degradation (29) support a protective role for the intranuclear sequestration of aberrant proteins (7). However, specific aggregation-prone proteins may escape recognition by the nuclear quality-control machinery. For example, nuclear aggregates of polyQ expansion proteins have been shown to interfere with transcriptional regulation by engaging transcription factors containing glutamine repeats (30). A better understanding of nuclear proteostasis may help in developing new strategies for the treatment of proteinopathies.

#### REFERENCES AND NOTES

1. E. T. Powers, R. I. Morimoto, A. Dillin, J. W. Kelly, W. E. Balch, *Annu. Rev. Biochem.* **78**, 959–991 (2009).
2. F. U. Hartl, A. Bracher, M. Hayer-Hartl, *Nature* **475**, 324–332 (2011).
3. R. C. Taylor, A. Dillin, *Cold Spring Harb. Perspect. Biol.* **3**, a004440 (2011).

4. T. P. Knowles, M. Vendruscolo, C. M. Dobson, *Nat. Rev. Mol. Cell Biol.* **15**, 384–396 (2014).
5. K. Y. Liu *et al.*, *Hum. Mol. Genet.* **24**, 1602–1616 (2015).
6. A. S. Hackam, R. Singaraja, T. Zhang, L. Gan, M. R. Hayden, *Hum. Mol. Genet.* **8**, 25–33 (1999).
7. F. Saudou, S. Finkbeiner, D. Devys, M. E. Greenberg, *Cell* **95**, 55–66 (1998).
8. M. W. West *et al.*, *Proc. Natl. Acad. Sci. U.S.A.* **96**, 11211–11216 (1999).
9. H. Olzscha *et al.*, *Cell* **144**, 67–78 (2011).
10. K. Zhang *et al.*, *Nature* **525**, 56–61 (2015).
11. R. Lalavade, N. Griesche, D. P. Ryan, S. Hildebrand, S. Krauss, *Cell Death Dis.* **4**, e752 (2013).
12. E. E. Nesterov *et al.*, *Angew. Chem. Int. Ed. Engl.* **44**, 5452–5456 (2005).
13. T. Jakhria *et al.*, *J. Biol. Chem.* **289**, 35781–35794 (2014).
14. W. Y. Chan *et al.*, *Biochemistry* **28**, 1033–1039 (1989).
15. A. Szebeni, M. O. Olson, *Protein Sci.* **8**, 905–912 (1999).
16. B. Wolff, J. J. Sanglier, Y. Wang, *Chem. Biol.* **4**, 139–147 (1997).
17. P. A. Baeuerle, D. Baltimore, *Cell* **53**, 211–217 (1988).
18. K. C. Carter, K. L. Taneja, J. B. Lawrence, *J. Cell Biol.* **115**, 1191–1202 (1991).
19. C. Yang *et al.*, *PLOS ONE* **5**, e15878 (2010).
20. L. Mangiarini *et al.*, *Cell* **87**, 493–506 (1996).
21. H. Li *et al.*, *Hum. Mol. Genet.* **8**, 1227–1236 (1999).
22. B. Bolognesi *et al.*, *ACS Chem. Biol.* **5**, 735–740 (2010).
23. N. Visa *et al.*, *Cell* **84**, 253–264 (1996).
24. H. Cheng *et al.*, *Cell* **127**, 1389–1400 (2006).
25. O. D. King, A. D. Gitler, J. Shorter, *Brain Res.* **1462**, 61–80 (2012).
26. B. Chi *et al.*, *Nucleic Acids Res.* **41**, 1294–1306 (2013).
27. B. D. Freibaum *et al.*, *Nature* **525**, 129–133 (2015).

28. A. Jovičić *et al.*, *Nat. Neurosci.* **18**, 1226–1229 (2015).
29. M. S. Hipp, S. H. Park, F. U. Hartl, *Trends Cell Biol.* **24**, 506–514 (2014).
30. K. L. Sugars, D. C. Rubinstein, *Trends Genet.* **19**, 233–238 (2003).

#### ACKNOWLEDGMENTS

We thank R. Klein, K. Schulz-Trieglaff, and I. Dudanova from the Max Planck Institute of Neurobiology for help with the preparation of primary neurons and brain slices, and J. Cox, F. Hosp, and M. Duerrbaum for support with proteomic data analysis. We thank C. Klaijs and D. Balchin for critically reading the manuscript. The research leading to these results has received funding from the European Commission under grant FP7 GA ERC-2012-SyG\_318987-ToPAG (to A.C.W., D.H., M.M., F.U.H., and M.S.H.), the Munich Cluster for Systems Neurology (K.F.W., M.M., F.U.H. and M.S.H.), the German Research Foundation (J.T., K.F.W.), and the Hans and Ilse Breuer Foundation (M.P.). F.U.H. has an advisory position with Proteostasis Therapeutics Inc. Data from the mass spectrometry analysis described in this manuscript can be found in the supplementary materials.

#### SUPPLEMENTARY MATERIALS

www.sciencemag.org/content/351/6269/173/suppl/DC1  
Materials and Methods  
Figs. S1 to S11  
Tables S1 to S3  
References (31–47)

7 August 2015; accepted 11 November 2015  
Published online 3 December 2015  
10.1126/science.aad2033

#### STEM CELL NICHE

## Fetal liver hematopoietic stem cell niches associate with portal vessels

Jalal A. Khan,<sup>1,2,5</sup> Avital Mendelson,<sup>1,2</sup> Yuya Kunisaki,<sup>1,2\*</sup> Alexander Birbrair,<sup>1,2</sup> Yan Kou,<sup>6</sup> Anna Arnal-Estapé,<sup>1,2†</sup> Sandra Pinho,<sup>1,2</sup> Paul Ciero,<sup>1</sup> Fumio Nakahara,<sup>1,2</sup> Avi Ma'ayan,<sup>6</sup> Aviv Bergman,<sup>4</sup> Miriam Merad,<sup>5</sup> Paul S. Frenette<sup>1,2,3‡</sup>

Whereas the cellular basis of the hematopoietic stem cell (HSC) niche in the bone marrow has been characterized, the nature of the fetal liver niche is not yet elucidated. We show that Nestin<sup>+</sup>NG2<sup>+</sup> pericytes associate with portal vessels, forming a niche promoting HSC expansion. Nestin<sup>+</sup>NG2<sup>+</sup> cells and HSCs scale during development with the fractal branching patterns of portal vessels, tributaries of the umbilical vein. After closure of the umbilical inlet at birth, portal vessels undergo a transition from Neuropilin-1<sup>+</sup>Ephrin-B2<sup>+</sup> artery to EphB4<sup>+</sup> vein phenotype, associated with a loss of periportal Nestin<sup>+</sup>NG2<sup>+</sup> cells and emigration of HSCs away from portal vessels. These data support a model in which HSCs are titrated against a periportal vascular niche with a fractal-like organization enabled by placental circulation.

**H**ematopoietic stem cells (HSCs) are generated in the mouse fetus around embryonic day 10.5 (E10.5) from hemogenic endothelium of the dorsal aorta (1, 2), then migrate to the placenta via the umbilical arteries (3) and return to the fetus via the umbilical vein (4). The umbilical vein delivers oxygenated blood to the fetus via the portal sinus, whose branches give rise to the portal vessels in the fetal liver (FL). In this organ, HSCs undergo marked expansion (5). The predictable growth curve of HSCs during development suggests that hitherto unknown determinants set the numbers of these cells.

Although FL HSCs are highly proliferative, a hallmark of adult bone marrow (BM) HSCs is their cell cycle quiescence (6). Perivascular cells expressing Nestin (7), CXCL12 (8), and the leptin

receptor (9) contribute to HSC maintenance. Nestin<sup>+</sup>NG2<sup>+</sup> arteriolar pericytes (10), as well as megakaryocytes (11, 12), maintain quiescent HSCs

<sup>1</sup>Ruth L. and David S. Gottesman Institute for Stem Cell and Regenerative Medicine Research, Albert Einstein College of Medicine, Bronx, NY, USA. <sup>2</sup>Department of Cell Biology, Albert Einstein College of Medicine, Bronx, NY, USA. <sup>3</sup>Department of Medicine, Albert Einstein College of Medicine, Bronx, NY, USA. <sup>4</sup>Department of Systems and Computational Biology, Albert Einstein College of Medicine, Bronx, NY, USA. <sup>5</sup>Department of Oncological Sciences, Icahn School of Medicine at Mount Sinai, New York, NY, USA. <sup>6</sup>Department of Pharmacology and Systems Therapeutics, Icahn School of Medicine at Mount Sinai, New York, NY, USA.

\*Present address: Department of Medicine and Biosystemic Science, Kyushu University, Fukuoka 812-8582, Japan. †Present address: Department of Pathology, Yale University School of Medicine, New Haven, CT 06510, USA. ‡Corresponding author. E-mail: paul.frenette@einstein.yu.edu

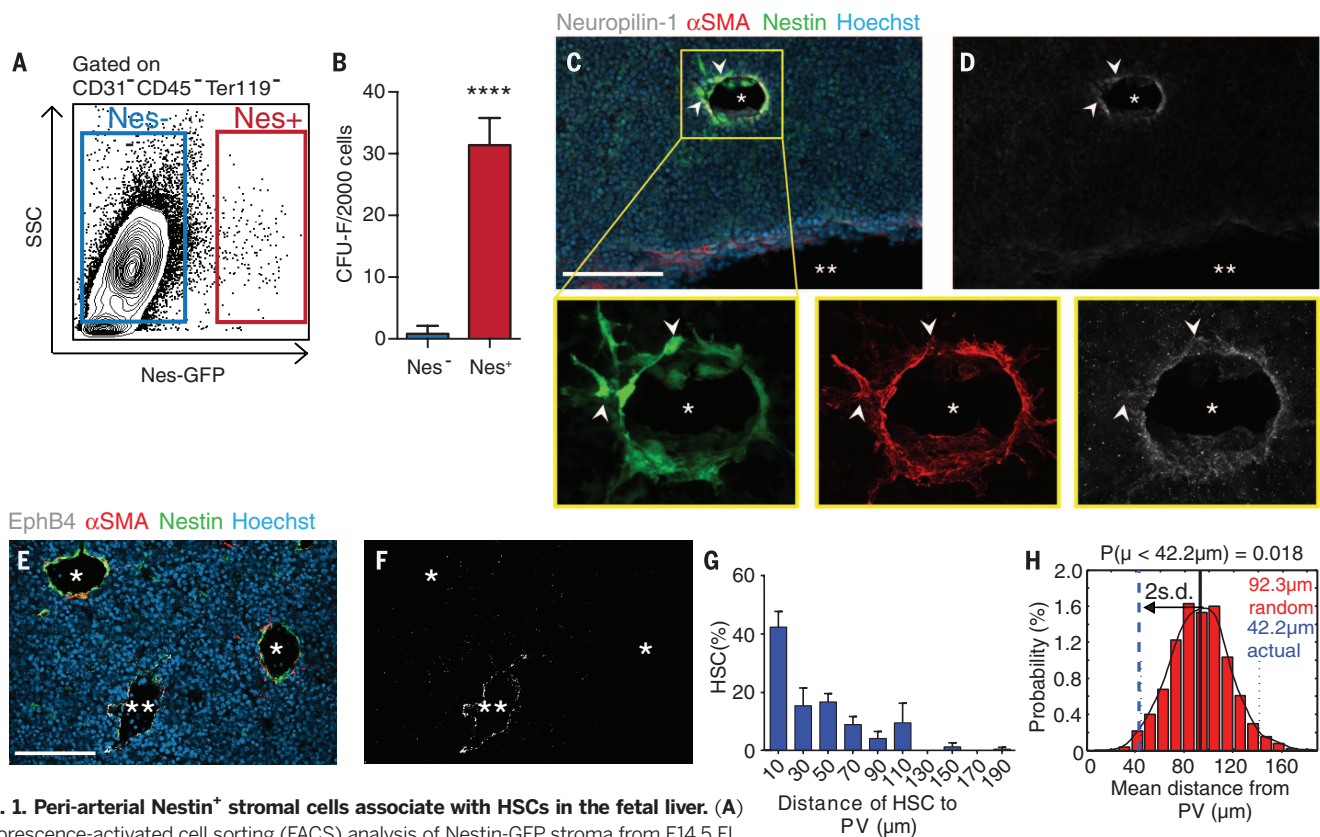


**Fig. 1. Peri-arterial Nestin<sup>+</sup> stromal cells associate with HSCs in the fetal liver.** (A) Fluorescence-activated cell sorting (FACS) analysis of Nestin-GFP stroma from E14.5 FL. (B) CFU-F from sorted FL cells;  $n = 4$ . (C to F) Immunofluorescence analyses of Nestin-GFP E14.5 FL cryosections stained for Neuropilin-1 [white, (C) and (D)] or EphB4 [white, (E) and (F)]. Colocalization of  $\alpha$ SMA<sup>+</sup> and Nestin<sup>+</sup> pericytes around Neuropilin-1<sup>+</sup> portal vessels (\*) but not EphB4<sup>+</sup> veins (\*\*). Scale bar, 100  $\mu$ m. (G) Distance distribution between CD150<sup>+</sup>CD48<sup>-</sup>CD41<sup>-</sup>Lineage<sup>-</sup> HSCs and Nestin<sup>+</sup> cells from whole-mount stained Nestin-GFP FL ( $n = 105$  from 12 E14.5 FLs), binned into 20- $\mu$ m intervals. (H) Probability distribution of mean distances from simulations of randomly positioned HSCs in relation to Nestin<sup>+</sup> cells. Actual mean distance shown in relation to mean of simulations  $\pm 2$  SD. \*\*\*\* $P < 10^{-4}$ .

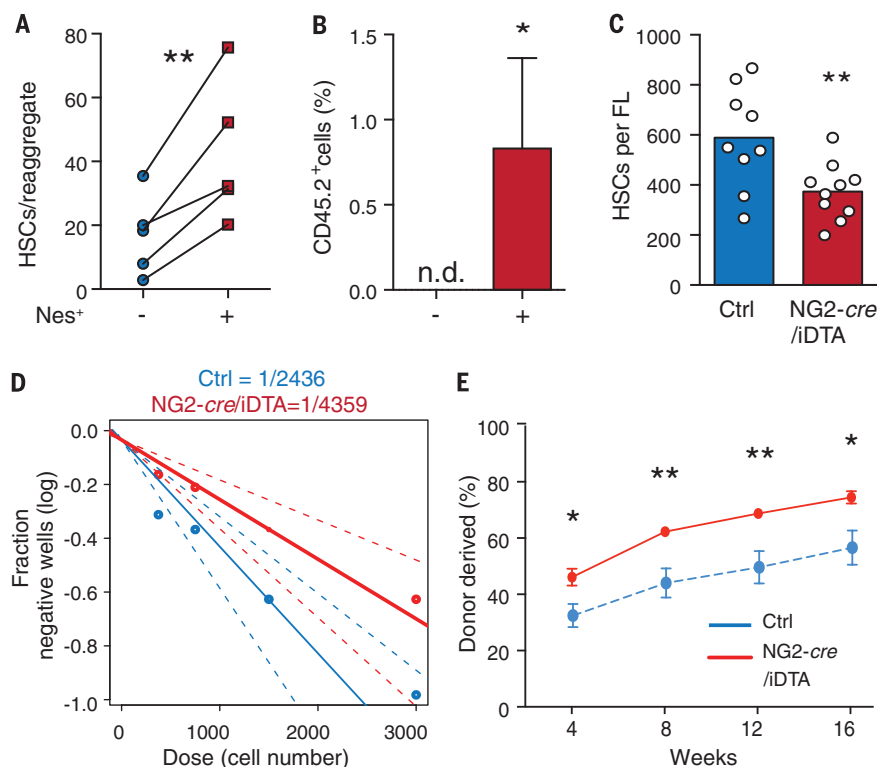


**Fig. 2. Nestin<sup>+</sup> perivascular cells drive HSC expansion in vivo.** (A) FACS quantification of CD150<sup>+</sup>Sca1<sup>+</sup> CD45<sup>+</sup> CD48<sup>-</sup>Lin<sup>-</sup> HSCs in reaggregates, with or without Nestin<sup>+</sup> cells. (B) Donor engraftment 16 weeks after transplantation of reaggregates together with congenic competitor cells. n.d., not detectable.  $n = 6$  to 7 per group. (C) CD150<sup>+</sup>CD48<sup>-</sup>Sca1<sup>+</sup>CD11b<sup>+</sup>CD45<sup>+</sup>CD41<sup>-</sup>Lineage<sup>-</sup> DAPI<sup>-</sup> HSC numbers in control and NG2-depleted littermates. (D) Limiting dilution analyses of LTC-ICs in Lineage<sup>-</sup> cells from NG2-depleted (red) and control (blue) littermate FLs. (E) Competitive repopulation assays of NG2-depleted and control FLs.  $n = 6$  and 7 mice per control and depleted littermates, respectively. \* $P < 0.05$ , \*\* $P < 0.01$ .

in the BM. Much less is known about the FL niche promoting HSC proliferation. FL-derived stromal cell lines support HSC expansion in vitro (13, 14). However, a HSC niche in the liver has not been demonstrated in vivo.

Within the E14.5 FL of Nestin-GFP (green fluorescent protein) transgenic mice, endothelial cells and a rare population of stromal cells (Fig. 1A) ( $0.045\% \pm 0.007\%$  of total nucleated cells) are marked by GFP. These stromal cells, hereafter termed Nestin<sup>+</sup> cells, are highly enriched in colony-forming unit–fibroblast activity (CFU-F) (Fig. 1B) and expressed mesenchymal lineage markers and DLK1, but neither the biliary marker EpCAM (15) nor hepatic genes (fig. S1, A and B). FL CFU-F colonies derived from Nestin<sup>+</sup> cells had trilineage mesenchymal lineage capacity when cultured in defined conditions (fig. S1, C to F). Nestin<sup>+</sup> cells expressed  $\alpha$ -smooth muscle actin ( $\alpha$ SMA) (fig. S1G), the pericyte marker NG2 (fig. S2, C and D), and colocalized with  $\alpha$ SMA staining on portal vessels expressing the endothelial arterial markers Ephrin-B2 and Neuropilin-1 but not the venular marker EphB4 (fig. S1, H to J, and Fig. 1, C to F). Thus, Nestin<sup>+</sup> cells are pericytes abutting *Efnb2* and Neuropilin-1-expressing endothelia on portal vessels. Last, Nestin<sup>+</sup> cells were enriched for HSC niche and expansion factors (fig. S1, K and L), raising the potential for regulating FL HSCs.

To evaluate the spatial relationships between HSCs and Nestin<sup>+</sup> cells, we stained CD150<sup>+</sup>CD48<sup>-</sup>CD41<sup>-</sup> Lineage<sup>-</sup> HSCs in whole-mount FLs and evaluated the significance of the associations by computational modeling (10). A large HSC fraction (>40%) was located within 20  $\mu$ m of Nestin<sup>+</sup> cells on portal vessels (Fig. 1G). We then sim-

ulated nonpreferential HSC placement on images of whole-mount prepared FLs to define the distribution of randomly localized HSCs to portal vessels. The observed HSC mean distance to Nestin<sup>+</sup> cells (42.2  $\mu$ m) was statistically different from that of randomly placed HSCs (92.3  $\mu$ m,  $P = 0.018$ ) (Fig. 1H). The close physical associations between HSCs and Nestin<sup>+</sup> periportal cells suggest that the portal vasculature may harbor a HSC niche.

We adapted the reaggregate organ culture assay in which selected populations are pelleted and cultured on the surface of a porous membrane (16). A FL cell mixture containing hematopoietic stem and progenitor cells (Lineage<sup>-</sup>CD45<sup>+</sup>), CD31<sup>+</sup> endothelial cells, and hepatic parenchymal/stromal cells (CD45<sup>-</sup> Lineage<sup>-</sup>) was separated by cell sorting and was reaggregated with or without Nestin<sup>+</sup> cells (ratio ~235/1) and cultured in the absence of exogenous cytokines or serum (fig. S2A). Significantly higher numbers of phenotypic HSCs (17) were maintained in the reaggregates containing Nestin<sup>+</sup> cells after 7 days in culture (Fig. 2A and fig. S2B), and these reaggregates contained detectable long-term repopulating FL HSC activity after transplantation, whereas the controls did not (Fig. 2B). These results suggest that factors produced by the FL Nestin<sup>+</sup> cells were sufficient to maintain HSCs in culture.

In contrast to Nestin-GFP, which also labels FL endothelial cells, NG2 expression was specific to Nestin<sup>+</sup> pericytes (~98% overlap) (fig. S2, C to G) and  $\alpha$ SMA<sup>+</sup> portal vessels, as determined by NG2-*cre* transgenic mice (18) crossed with inducible TdTomato transgenic mice (fig. S2, H and I). We then crossed male NG2-*cre* mice with female Cre-inducible diphtheria toxin A (iDTA) mice to

deplete NG2<sup>+</sup> cells by selective expression of DTA after NG2-*cre*-mediated excision of a floxed-STOP cassette (19). Embryos were staged in utero by crown-rump length (CRL) using ultrasound imaging (fig. S2J). NG2-*cre*/iDTA fetuses did not exhibit gross developmental defects compared with littermates (fig. S3A) and had similar CRL (fig. S3B). Although NG2-*cre* activity was detected in mural cells surrounding the midline dorsal aorta at E11 (fig. S3C), we found no difference in HSCs and LSKs in E12 to E12.5 FLs of NG2-*cre*/iDTA transgenic mice (fig. S3, D to G), suggesting that HSC specification and homing to FL were not significantly altered. At E14.5, however, HSCs were significantly reduced (by ~45%) (Fig. 2C and fig. S3H) in FLs from NG2-*cre*/iDTA fetuses compared with control littermates, whereas progenitors were unaffected (fig. S3, I and J). Limiting dilution analyses also revealed a 45% reduction of long-term culture–initiating colonies (LTC-IC) (20) in NG2-*cre*/iDTA FLs compared with control littermates (Fig. 2D). These data suggest that Nestin<sup>+</sup>NG2<sup>+</sup> cells provide a niche in the FL.

HSCs from NG2-*cre*/iDTA mice FLs exhibited reductions (~43%) in bromodeoxyuridine uptake compared with littermate controls, suggesting that Nestin<sup>+</sup>NG2<sup>+</sup> cells are required for HSC proliferation (fig. S3K). Consistent with previous reports suggesting a reduced capacity of S/G<sub>0</sub>/M-phase HSCs to engraft irradiated recipient mice (20, 21), we observed an increase in HSC engraftment in NG2-*cre*/iDTA FLs compared with control littermates (Fig. 2E and fig. S4A). Indeed, engraftment-competent G<sub>0</sub>/G<sub>1</sub>-phase HSCs were enriched in NG2-*cre*/iDTA mice compared with littermate controls, whereas the S/G<sub>0</sub>/M-phase HSCs (DNA > 2n)

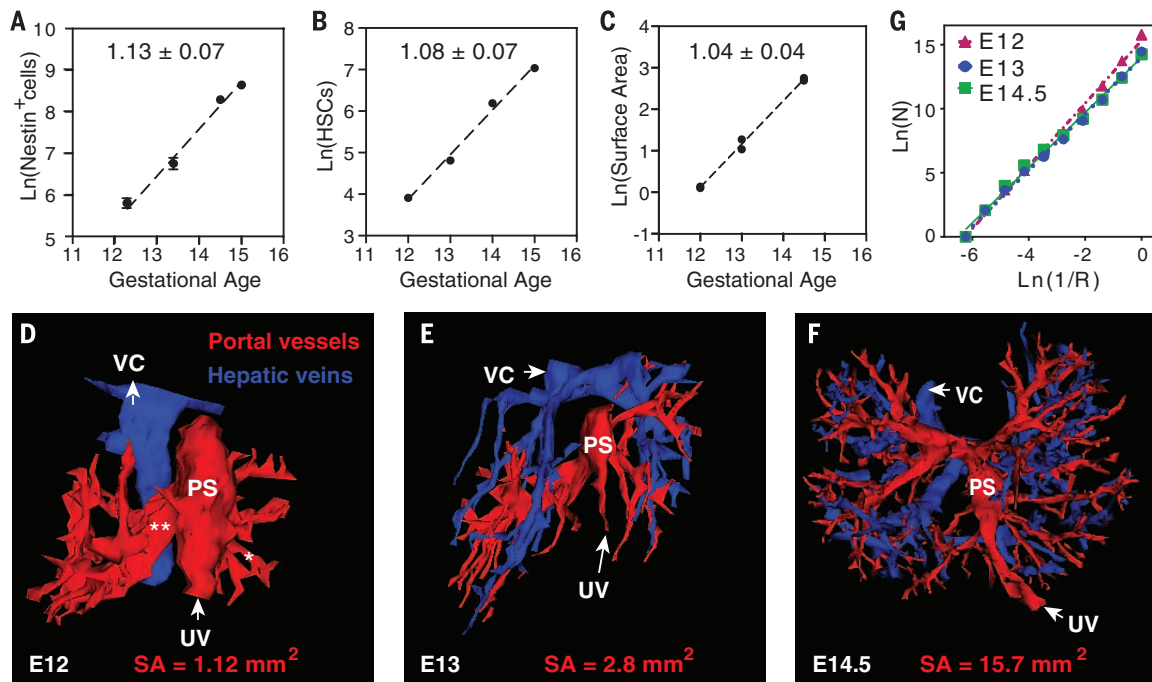


**Fig. 3. Fractal geometry underlies HSC expansion.** (A) Nestin<sup>+</sup> cells expand from E12 to E15 according to a power law ( $R^2 = 0.95$ ). (B) HSC numbers relative to gestational age plotted from quantification of Ema *et al.* (5). (C) Portal vessel surface area from E12 to E14.5 scales according to a similar power law ( $R^2 = 0.99$ ;  $n = 6$ ). Slopes indicated in panels. (D to F) 3D reconstructions of afferent PVs (red) and efferent veins (blue) in E12 (D), E13 (E), and E14.5 (F) FLs. PS, portal sinus; VC, vena cava; SA, surface area. (G) Calculation of the scale-invariant fractal dimension of FL afferent vessels using box-counting.

were reduced (fig. S4, B to F). Together, these data indicate that Nestin<sup>+</sup> cells are required to drive fetal HSC expansion.

Because arteriole-associated Nestin<sup>+</sup>NG2<sup>+</sup> cells promote HSC quiescence in adult BM (10) and analogous cells appear to exert opposite functions in the FL, we next sequenced cDNA libraries of Nestin<sup>+</sup>NG2<sup>+</sup> cells sorted from BM and FL stroma from Nestin-GFP;NG2-DsRed double-transgenic mice (fig. S5). Most (95.6%) BM and FL Nestin<sup>+</sup>NG2<sup>+</sup> cell transcripts were statistically indistinguishable, but FL transcripts accounted for the majority of differentially expressed (DE) genes (fig. S5, A and B), suggesting that these cells are highly similar. Indeed, BM and FL Nestin<sup>+</sup>NG2<sup>+</sup> cells had similar expression of many HSC niche and pericyte genes (fig. S5, F and H). Accordingly, reaggregation of E14.5 FL cell mixtures with similar numbers of adult BM Nestin<sup>bright</sup> cells (10) or FL Nestin<sup>+</sup> cells revealed a similar capacity to support HSCs (fig. S4G). In addition, *Scf*, *Angptl2*, and *Igf2* expression in Nestin<sup>+</sup> cells were similar

at E12, E13, and E14.5, suggesting that Nestin<sup>+</sup> cells do not expand HSCs by increasing expression of these factors (fig. S4, H and I). FL DE genes were analyzed with the Enrichr gene-set enrichment analysis tool (22); genes involved in mitosis, metabolism, and growth—as well as knockout phenotypes including abnormal blood vessel development, blood circulation, and cell proliferation—were significantly enriched (fig. S5, C to E). Chromatin immunoprecipitation sequencing enrichment analyses (23) applied to identify upstream regulatory factors highly connected to FL DE genes pointed to key drivers of cell cycle progression (fig. S6, A to C). Accordingly, FL Nestin<sup>+</sup> cells differentially expressed cell cycle genes, including *Ki67*, and were actively proliferating (figs. S5I and S1M).

The enrichment of genes promoting cell cycle progression and vascular development supports the hypothesis—as implied by the niche concept—that the expansion of Nestin<sup>+</sup>NG2<sup>+</sup> cells and portal vessels is synchronized with HSC expansion. The absolute numbers of Nestin<sup>+</sup> cells increased loga-

rithmically over E12 to E14.5 (Fig. 3A). When compared with numbers of HSCs (Fig. 3B) (5), the rates of expansion were indistinguishable (Fig. 3, A and B) [ $P = 0.69$ , analysis of covariance (ANCOVA)]. We next mapped the vasculature by tracing vessels in consecutive cryosections of Nestin-GFP<sup>+</sup> FLs from E12 to E14.5 (fig. S7, A to C) to generate complete three-dimensional (3D) surface maps (Fig. 3, D to F). Portal vessels receiving blood from the umbilical vein (UV) were lined with Nestin<sup>+</sup> cells (fig. S7, A to C, and Fig. 3, D to F), in contrast to  $\alpha$ SMA-negative hepatic veins that lacked Nestin<sup>+</sup> cell lining (fig. S7C). At E13 and E14.5, portal vessel branching became progressively more intricate (Fig. 3, E and F), and the surface area of these structures increased logarithmically. Nestin<sup>+</sup> cell numbers and portal vessels' surface area scaled over time with indistinguishable slopes ( $P = 0.47$ , ANCOVA) (Fig. 3, A and C), suggesting that the HSC niche expansion is also related to portal vessel surface area.

That Nestin<sup>+</sup> cell and portal vessel expansion fit a power law suggests that they follow a fractal-like

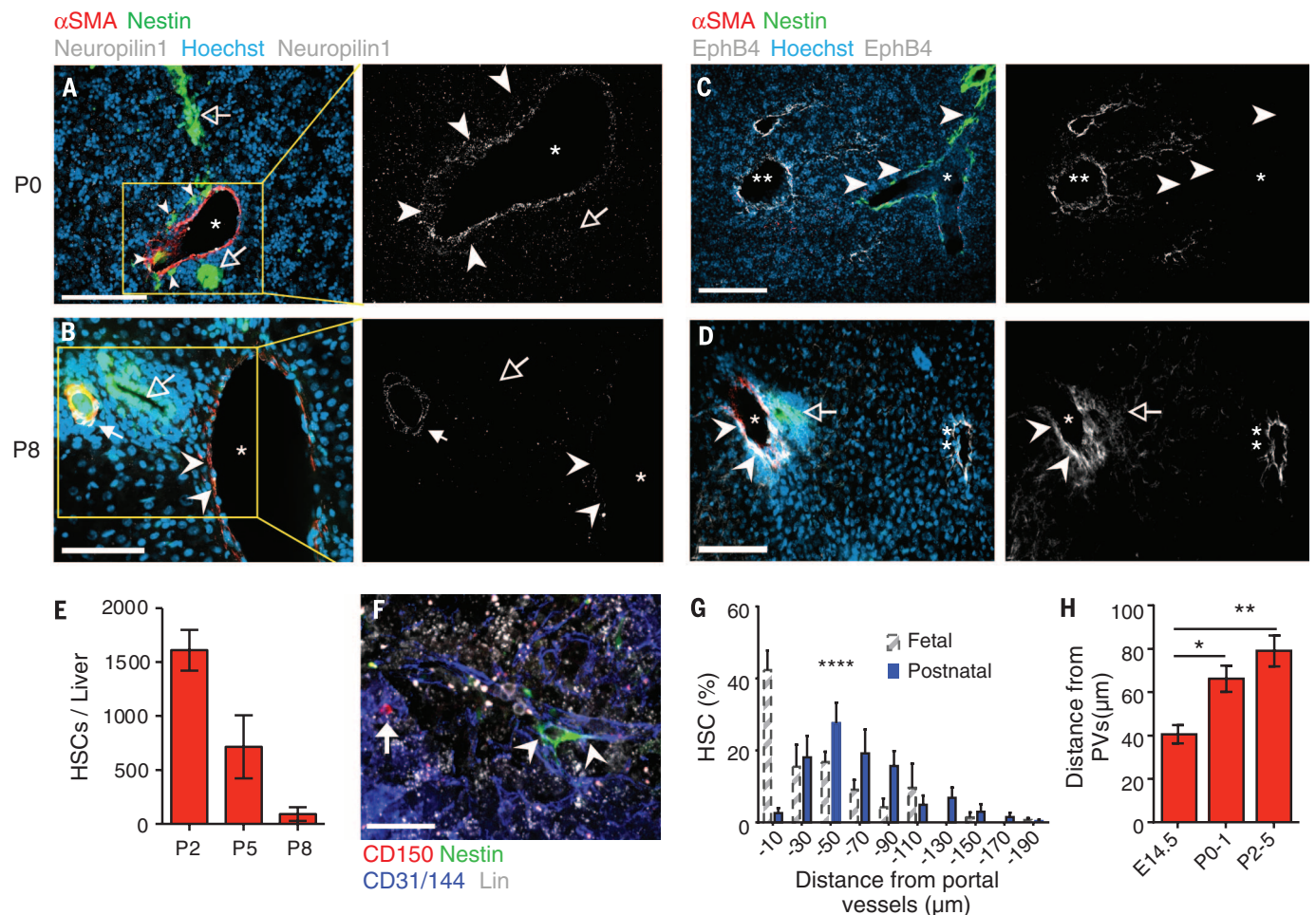


**Fig. 4. Ligation of the umbilical vein inlet terminates the portal vessel HSC niche.** (A to D) Immunofluorescence analyses of P0 [(A) and (C)] and P8 [(B) and (D)] liver cryosections stained for  $\alpha$ SMA (red), Nestin-GFP (green), nuclear dye Hoechst (blue), and Neuropilin-1 or EphB4 (white). \*, portal vessels; \*\*, hepatic veins; arrowheads, Nestin<sup>+</sup> cells (P0) or outline of portal vessel; solid arrow, hepatic artery; open arrows, bile ducts. (E) FACS analysis showing decreasing numbers of CD150<sup>+</sup>CD48<sup>+</sup>Sca1<sup>+</sup>CD11b<sup>+</sup>CD45<sup>+</sup>CD41<sup>-</sup>Lineage<sup>-</sup>DAPI<sup>-</sup>

HSCs between P2 and P8. (F) Representative whole-mount immunofluorescence imaging of a CD150<sup>+</sup>CD48<sup>-</sup>Lin<sup>-</sup> HSC (arrow) in P3 fetal liver. Arrowheads, portal vessel. (G) Distance distribution of HSCs from portal vessels ( $n = 77$  from 20 livers). FL HSC measurements from Fig. 1G (dashed-line bars) are shown for comparison. (H) HSC distances from portal vessels in fetal and postnatal livers showing increasing mean distances with age. Scale bars: (A) to (D), 100  $\mu$ m; F, 20  $\mu$ m. \* $P < 0.05$ , \*\* $P < 0.01$ , \*\*\*\* $P < 0.0001$ .

organization. Fractals are geometries exhibiting self-similarity; the observed structures share characteristics across spatial levels (24). To characterize the multiscale behavior of portal vessels, we applied a 3D box-counting algorithm. This method consists of overlaying the object with a series of 3D grids of exponentially decreasing block sizes ( $R$ ) and counting the number of boxes intersecting the object ( $N$ ). By analyzing the slope of  $N$  plotted against  $R^{-1}$  on a bilogarithmic scale, the dimensionality of the object was determined. Box-counting analysis revealed that portal vessels were self-similar over three decades of scale. Furthermore, the dimensionality was relatively constant as portal vessels branched over E12 to E14.5 (2.15 to 2.35) (Fig. 3G). These findings suggest that the expansion of HSCs and Nestin<sup>+</sup> cells during fetal development is governed by fractal-like geometries of the portal vessel niche.

After birth, ligation of the umbilical inlet leads to dramatic hemodynamic changes in portal vessel flow (fig. S8, A to E). Whereas at postnatal day 0 (P0), portal vessels expressed the arterial markers Neuropilin-1 and Ephrin-B2 and were accompanied by Nestin<sup>+</sup> cells (Fig. 4A and fig. S8F), their expression levels were markedly reduced in P8 portal vessels, which were, by then, devoid of Nestin<sup>+</sup> cells (Fig. 4B and fig. S8G), in part due to Nestin<sup>+</sup> cell apoptosis as detected by terminal deoxynucleotidyl transferase-mediated deoxyuridine triphosphate nick end labeling staining (fig. S8, H and I). At this time, portal vessels expressed EphB4 (Fig. 4, C and D), suggesting that they transited into a vein phenotype.

These notable changes were associated with a marked reduction in liver HSC content at P8 (Fig. 4E). Perinatal HSCs were also rapidly established in the neonatal spleen (fig. S8J) and might also contribute to sustaining blood production until the BM becomes fully functional (25, 26). Using whole-mount imaging, we found that, in contrast to the fetal liver, few HSCs (<3%) were located within 20  $\mu$ m of postnatal portal vessels (P0 to P5) (Fig. 4, F and G), and mean HSC distances to portal vessels increased significantly (Fig. 4H). These results thus further underscore the critical role for the arterial portal vessels in forming a FL niche.

Our data support the concept that HSCs are titrated against a branching portal vessel network. Fractal geometries of vessel branching optimize the delivery of blood (27), with each division serving a smaller compartment within the organ. The availability of niche cells to sustain proliferating HSCs may thus be tied to the innate growth of the portal vascular tree. Our results also provide a biological explanation for the rapid loss of HSCs in the postnatal liver, where dramatic postnatal changes in portal vessels lead to a loss of niche cells and the migration of HSCs away from the portal niche. As HSCs emerge from the largest artery (aorta), expand around arterial portal vessels of the fetal liver, and are later maintained quiescent in the adult marrow near small arterioles (10, 11), the arterial vasculature may provide an adaptive niche, serving hematopoiesis at multiple stages of mammalian life.

## REFERENCES AND NOTES

1. A. Medvinsky, E. Dzierzak, *Cell* **86**, 897–906 (1996).
2. J. C. Boisset *et al.*, *Nature* **464**, 116–120 (2010).
3. M. F. de Bruijn, N. A. Speck, M. C. Peeters, E. Dzierzak, *EMBO J.* **19**, 2465–2474 (2000).
4. C. Gekas, F. Dieterlen-Lièvre, S. H. Orkin, H. K. A. Mikkola, *Dev. Cell* **8**, 365–375 (2005).
5. H. Erma, H. Nakauchi, *Blood* **95**, 2284–2288 (2000).
6. A. Wilson *et al.*, *Cell* **135**, 1118–1129 (2008).
7. S. Méndez-Ferrer *et al.*, *Nature* **466**, 829–834 (2010).
8. A. Greenbaum *et al.*, *Nature* **495**, 227–230 (2013).
9. L. Ding, T. L. Saunders, G. Enikolopov, S. J. Morrison, *Nature* **481**, 457–462 (2012).
10. Y. Kunisaki *et al.*, *Nature* **502**, 637–643 (2013).
11. I. Bruns *et al.*, *Nat. Med.* **20**, 1315–1320 (2014).
12. M. Zhao *et al.*, *Nat. Med.* **20**, 1321–1326 (2014).
13. K. A. Moore, B. Pytowski, L. Witte, D. Hicklin, I. R. Lemischka, *Proc. Natl. Acad. Sci. U.S.A.* **94**, 4011–4016 (1997).
14. S. Chou, H. F. Lodish, *Proc. Natl. Acad. Sci. U.S.A.* **107**, 7799–7804 (2010).
15. M. Tanaka *et al.*, *Mech. Dev.* **126**, 665–676 (2009).
16. J. M. Sheridan, S. Taoudi, A. Medvinsky, C. C. Blackburn, *Genesis* **47**, 346–351 (2009).
17. I. Kim, S. He, O. H. Yilmaz, M. J. Kiel, S. J. Morrison, *Blood* **108**, 737–744 (2006).
18. X. Zhu, D. E. Bergles, A. Nishiyama, *Development* **135**, 145–157 (2008).
19. D. Voehringer, H. E. Liang, R. M. Locksley, *J. Immunol.* **180**, 4742–4753 (2008).
20. M. B. Bowie, D. G. Kent, M. R. Copley, C. J. Eaves, *Blood* **109**, 5043–5048 (2007).
21. E. Passequé, A. J. Wagers, S. Giuriato, W. C. Anderson, I. L. Weissman, *J. Exp. Med.* **202**, 1599–1611 (2005).
22. E. Y. Chen *et al.*, *BMC Bioinformatics* **14**, 128 (2013).
23. A. Lachmann *et al.*, *Bioinformatics* **26**, 2438–2444 (2010).
24. A. L. Goldberg *et al.*, *Proc. Natl. Acad. Sci. U.S.A.* **99** (suppl. 1), 2466–2472 (2002).
25. J. L. Christensen, D. E. Wright, A. J. Wagers, I. L. Weissman, *PLOS Biol.* **2**, e75 (2004).
26. F. M. Wolber *et al.*, *Exp. Hematol.* **30**, 1010–1019 (2002).
27. H. K. Hahn, M. Georg, H.-O. Peitgen, in *Fractals in Biology and Medicine*, G. A. Losa, D. Merlini, T. F. Nonnenmacher, E. R. Weibel, Eds. (Birkhäuser, 2005), pp. 55–66.

## ACKNOWLEDGMENTS

We are grateful to the National Institutes of Health (NIH) for support: Integrated Training in Pharmacological Science program (NIGMS T32 063754) and National Heart, Lung, and Blood Institute (NHLBI) Ruth L. Kirschstein National Research Service Award (NRSA) predoctoral M.D./Ph.D. fellowship (F30 943257) to J.A.K.; NHLBI Ruth L. Kirschstein NRSA postdoctoral fellowship F32 HL123224 to A.Me.; R01 grants HL097700, DK056638, and HL069438 to P.S.F.; and R01 grants CA164468 and DA033788 to A.Be. S.P. is a New York Stem Cell Foundation–Druckenmiller Fellow. A.Ma. is supported by U54HL127624, U54CA189201, and RO1GM098316. We thank A. L. Kolodkin for providing antibody to Nrpl and L. Silberstein for RNA-sequencing recommendations. We thank O. Uche and L. Tesfa for technical assistance with sorting and K. O'Connell for technical assistance with Vevo Ultrasound imaging technology. We are also grateful to the New York State Department of Health (NYSTEM Program) for shared facility (C029154) and research support (N13G-262). This work was funded by NIH grants R01 DK056638, R01 HL116340, R01 HL069438, and NYSTEM grants (C029154 and C029570). J.A.K. designed and analyzed experiments in this study. Y.Ku. performed transplantations. J.A.K. and Y.Ku. performed the in vivo experiments. J.A.K., Y.Ku., and A.Me. performed whole-mount experiments; J.A.K., A.A.-E., P.C., A.Me., and A.Bi. performed immunostaining. J.A.K. and S.P. performed the LTC-IC experiments; A.Me. and S.P. performed differentiation assays; J.A.K., F.N., and A.Me. performed expression analyses; J.A.K. performed the RNA-sequencing experiments; Y.Ko., A.Ma., and J.A.K. analyzed the RNA-sequencing data; J.A.K. and A.Be. performed computational modeling and statistical analysis of the data; and J.A.K. and P.S.F. wrote the manuscript. The authors declare no competing financial interests.

## SUPPLEMENTARY MATERIALS

www.sciencemag.org/content/351/6269/176/suppl/DC1  
Materials and Methods  
Figs. S1 to S8  
Table S1  
References (28–39)

12 July 2015; accepted 15 September 2015  
Published online 3 December 2015  
10.1126/science.aad0084

## PROTEIN STRUCTURE

## The structure of the $\beta$ -barrel assembly machinery complex

Jeremy Bakelar,<sup>1</sup> Susan K. Buchanan,<sup>2</sup> Nicholas Noinaj<sup>1\*</sup>

$\beta$ -Barrel outer membrane proteins (OMPs) are found in the outer membranes of Gram-negative bacteria and are essential for nutrient import, signaling, and adhesion. A 200-kilodalton five-component complex called the  $\beta$ -barrel assembly machinery (BAM) complex has been implicated in the biogenesis of OMPs. We report the structure of the BAM complex from *Escherichia coli*, revealing that binding of BamCDE modulates the conformation of BamA, the central component, which may serve to regulate the BAM complex. The periplasmic domain of BamA was in a closed state that prevents access to the barrel lumen, which indicates substrate OMPs may not be threaded through the barrel during biogenesis. Further, conformational shifts in the barrel domain lead to opening of the exit pore and rearrangement at the lateral gate.

Gram-negative bacteria contain both an inner membrane (IM) and an outer membrane (OM) that serve important roles in nutrient import, cell signaling, waste export, and protection. Integral membrane proteins in the IM all have an  $\alpha$ -helical fold consisting of one or more  $\alpha$ -helices. In the OM, however, integral membrane proteins have a  $\beta$ -barrel

fold consisting of 8 to 26 antiparallel  $\beta$ -strands. In pathogenic strains of bacteria, some outer membrane proteins (OMPs) can also serve as

<sup>1</sup>Markey Center for Structural Biology, Department of Biological Sciences, Purdue University, West Lafayette, IN 47907, USA.

<sup>2</sup>National Institute of Diabetes and Digestive and Kidney Diseases, National Institutes of Health, Bethesda, MD 20892, USA.

\*Corresponding author. E-mail: nnoinaj@purdue.edu

EXTENDED PDF FORMAT  
SPONSORED BY



### Fetal liver hematopoietic stem cell niches associate with portal vessels

Jalal A. Khan, Avital Mendelson, Yuya Kunisaki, Alexander Birbrair, Yan Kou, Anna Arnal-Estapé, Sandra Pinho, Paul Ciero, Fumio Nakahara, Avi Ma'ayan, Aviv Bergman, Miriam Merad and Paul S. Frenette (December 3, 2015)  
*Science* **351** (6269), 176-180. [doi: 10.1126/science.aad0084]  
originally published online December 3, 2015

Editor's Summary

#### How HSCs populate the fetal liver

Hematopoietic stem cells (HSCs) undergo dramatic expansion in the fetal liver before migrating to their definitive site in the bone marrow. Khan *et al.* identify portal vessel-associated Nestin<sup>+</sup>NG2<sup>+</sup> pericytes as critical HSC niche components (see the Perspective by Cabezas-Wallscheid and Trumpp). The portal vessel niche and HSCs expand according to fractal geometries, suggesting that niche cells—rather than factors expressed by the niche—drive HSC proliferation. After birth, arterial portal vessels transform into portal veins, and lose Nestin<sup>+</sup>NG2<sup>+</sup> pericytes. When this happens, the niche is lost and HSCs migrate away from the neonatal liver.

*Science*, this issue p. 176; see also p. 126

---

This copy is for your personal, non-commercial use only.

---

**Article Tools** Visit the online version of this article to access the personalization and article tools:  
<http://science.sciencemag.org/content/351/6269/176>

**Permissions** Obtain information about reproducing this article:  
<http://www.sciencemag.org/about/permissions.dtl>

*Science* (print ISSN 0036-8075; online ISSN 1095-9203) is published weekly, except the last week in December, by the American Association for the Advancement of Science, 1200 New York Avenue NW, Washington, DC 20005. Copyright 2016 by the American Association for the Advancement of Science; all rights reserved. The title *Science* is a registered trademark of AAAS.